GDCh

Research Articles

Angewandte
Chemie
International Edition
www.angewandte.org

Perovskite Solar Cells Hot Paper

Tailoring Phase Alignment and Interfaces via Polyelectrolyte Anchoring Enables Large-Area 2D Perovskite Solar Cells

Chenxu Han, Yao Wang, Jiabei Yuan, Jianguo Sun, Xuliang Zhang, Claudio Cazorla, Xianxin Wu, Ziang Wu, Junwei Shi, Junjun Guo, Hehe Huang, Long Hu, Xinfeng Liu, Han Young Woo, Jianyu Yuan,* and Wanli Ma

Abstract: Ruddlesden–Popper phase 2D perovskite solar cells (PSCs) exhibit improved lifetime while still facing challenges such as phase alignment and up-scaling to module-level devices. Herein, polyelectrolytes are explored to tackle this issue. The contact between perovskite and hole-transport layer (HTL) is important for decreasing interfacial non-radiative recombination and scalable fabrication of uniform 2D perovskite films. Through exploring compatible butylamine cations, we first demonstrate poly(3-(4-carboxybutyl)thiophene-2,5-diyl)-butylamine (P3CT-BA) as an efficient HTL for 2D PSCs due to its great hydrophilicity, relatively high hole mobility and uniform surface. More importantly, the tailored P3CT-BA has an anchoring effect and acts as the buried passivator for 2D perovskites. Consequently, a best efficiency approaching 18 % was achieved and we further first report large-area (2×3 cm^2, 5×5 cm^2) 2D perovskite minimodules with an impressive efficiency of 14.81 % and 11.13 %, respectively.

Introduction

Two-dimensional (2D) metal halide perovskites with unique layered structure have recently attracted extensive research interest as promising materials for high-efficiency and long-term operationally stable perovskite solar cells (PSCs).[1–3] In comparison with three-dimensional (3D) organic–inorganic hybrid perovskites, the 2D perovskites share a general chemical composition of L$_2$A$_{n-1}$Pb$_n$X$_{3n+1}$ ($n = 1, 2, 3, 4…$), where L is a large organic cation (spacer).[4–6] On the basis of organic spacer type, a further classification commonly used divides them into Ruddlesden–Popper (RP), Dion–Jacobson (DJ) and alternating cations in the interlayer space (ACI) perovskites.[7–9] Among them, RP phase 2D halide perovskites of low $\langle n \rangle$ value (≤ 4) have been reported with improved stability towards humidity and light and higher chemical versatility, showing a power conversion efficiency (PCE) over 18 %,[10] making them promising alternatives for commercialization of PSCs.[11,12]

Despite this rapid progress, so far, the reported strategies for the successful fabrication of 2D perovskite films over large-area are very limited relative to their 3D counterparts. There are several issues that may limit the up-scaling to module-level devices of 2D PSCs. Firstly, layered perovskites deposited using solution methods typically suffer from a mixture of quantum wells with multiple $\langle n \rangle$ value distribution, which has severely hindered charge transport and induced additional energy losses when up-scaling to large-area devices.[13–15] Moreover, the addition of organic spacer cations significantly alters the precursor component interaction and coordination, which fundamentally change the crystallization process, and thus the kinetics of film formation is quite different compared to 3D analogues.[16–19] Furthermore, the top and buried contacts of 2D perovskites and interfacial transporting layer is less explored, which is

[*] C. Han, Dr. Y. Wang, J. Yuan, J. Sun, Dr. X. Zhang, J. Shi, J. Guo, H. Huang, Prof. J. Yuan, Prof. W. Ma
Institute of Functional Nano & Soft Materials (FUNSOM), Jiangsu Key Laboratory for Carbon-Based Functional Materials and Devices, Soochow University
199 Ren-Ai Road, Suzhou Industrial Park, Suzhou, Jiangsu 215123 (P. R. China)
E-mail: jyyuan@suda.edu.cn

Dr. C. Cazorla
Departament de Física, Universitat Politècnica de Catalunya
Campus Nord B4–B5, 08034 Barcelona (Spain)

X. Wu, Prof. X. Liu
CAS Key Laboratory of Standardization and Measurement for Nanotechnology, CAS Center for Excellence in Nanoscience, National Center for Nanoscience and Technology, Chinese Academy of Sciences
Beijing, 100190 (P. R. China)

Z. Wu, Prof. H. Y. Woo
Department of Chemistry, Korea University
Seoul, 02841 (Republic of Korea)

Dr. L. Hu
School of Engineering, Macquarie University
Sydney, New South Wales, 2109 (Australia)

Prof. X. Liu
Dalian National Laboratory for Clean Energy
Dalian 116023 (China)

Prof. J. Yuan, Prof. W. Ma
Jiangsu Key Laboratory of Advanced Negative Carbon Technologies, Soochow University
199 Ren-Ai Road, Suzhou Industrial Park, Suzhou, Jiangsu 215123 (P. R. China)

essential for efficient charge transfer and carrier extraction in large-area devices.[20,21] Therefore, the scalable deposition of a uniform 2D perovskite film currently remains both a key scientific and technical challenge.

In this work, we first propose a strategy via well-defined 2D perovskites/interfaces interaction to realize modified crystallization and growth to achieve a large-area and uniform 2D RP ($\langle n \rangle = 4$) phase perovskite film benefiting from conjugated polyelectrolytes poly(3-(4-carboxybutyl)-thiophene-2,5-diyl) (P3CT). Through tuning the functional cation to more compatible butylamine (BA), combined theoretical and experimental results confirmed P3CT-BA as a highly efficient hole-transporting layer (HTL) due to its great hydrophilicity, high hole mobility and more uniform surface. More importantly, the tailored P3CT-BA also has an anchoring effect and acts as the buried passivator for $BA_2MA_3Pb_4I_{13}$ 2D perovskite. Finally, a champion efficiency approaching 18% was achieved for small size 2D RP PSCs with excellent stability. More importantly, we first realize high-performance large-area 2D perovskites on a substrate of 2×3 cm^2 and 5×5 cm^2 (active area of 1 cm^2 and 16 cm^2), respectively.

Results and Discussion

P3CT was normally mixed with excess potassium hydroxide (KOH) to prepare an aqueous solution for depositing the HTL. The P3CT-BA aqueous solution was synthesized using a similar method, which incorporates BA instead of KOH. The P3CT-K and P3CT-BA HTL were fabricated under ambient conditions through a spin-coating process.[22–24] For the absorbing layer, the typical RP phase $BA_2MA_3Pb_4I_{13}$ 2D perovskite film was deposited on top of the P3CT-X by a hot spin-coating method using the parameters from a previous report.[14,25,26] We first compared the properties of P3CT with different cations as well as the RP phase $BA_2MA_3Pb_4I_{13}$ perovskite film coated on top of them. The molecular structures of P3CT-K and P3CT-BA are shown in Figure 1a, and the aqueous solutions exhibit different colors at the same concentration (2 mg mL^{-1}). Figure 1b provides the absorption spectra of both solutions, the P3CT-K solution shows a shoulder absorption peak around 600 nm, and the absorption spectra exhibits a ≈ 20 nm red-shift compared to that of P3CT-BA, indicating a higher degree of polymer aggregation for the P3CT-K solution.[27] Figure 1c
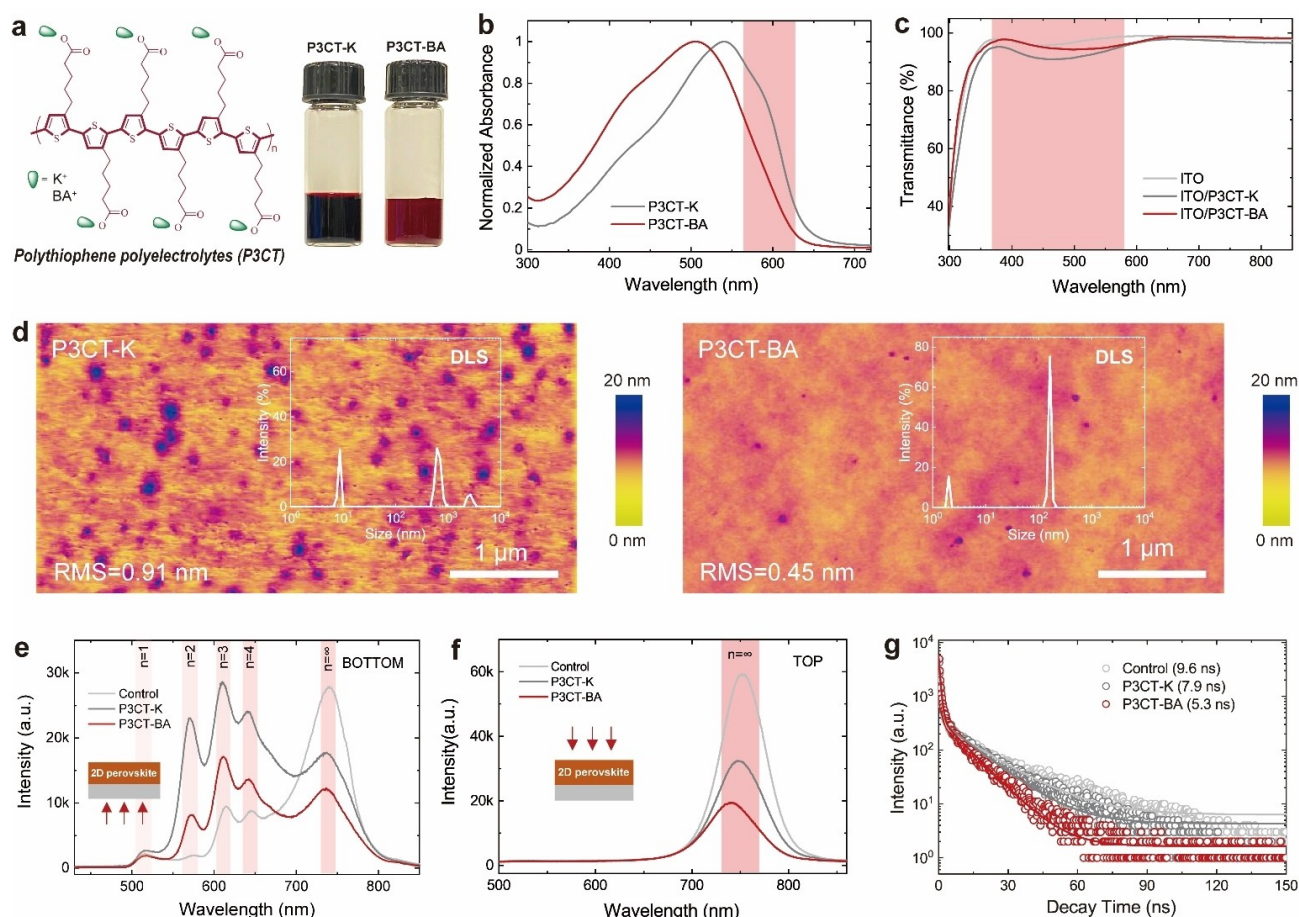
Figure 1. a) The molecular structures and aqueous solutions of P3CT-K and P3CT-BA. b) UV-vis absorption spectra of P3CT-K and P3CT-BA aqueous solutions. c) Transparency of the ITO, ITO/P3CT-K and ITO/P3CT-BA films. d) AFM height images of P3CT-K and P3CT-BA films (inset: DLS spectra of P3CT-K and P3CT-BA aqueous solution). e), f) Steady-state PL spectra of 2D perovskite films based on P3CT-K and P3CT-BA in both bottom and top excitation configurations. g) Time-resolved PL spectra of P3CT-K and P3CT-BA based 2D perovskite films.

Angew. Chem. Int. Ed. **2022**, e202205111 (2 of 10)

© 2022 Wiley-VCH GmbH

presents the transmittance spectra of P3CT-K and P3CT-BA films spin-coated on indium-tin-oxide (ITO) substrates. Bare ITO is also included for comparison. In comparison with P3CT-K, P3CT-BA shows higher transmittance in the range of 350–550 nm, which may be attributed to the different surface morphology. To understand the difference, a set of characterizations were further performed. Dynamic light scattering (DLS) and zeta potential were introduced to detect the polymer aggregate size distribution in the solution. As shown in Figure 1d, the particles were widely distributed in the P3CT-K solution, with separation varying from 10 nm to thousands of nanometers. Surprisingly, in the P3CT-BA solution, the particles show a narrow size distribution (1–100 nm). Moreover, the zeta potential results (Figure S1) show that the P3CT-BA solution possesses a larger absolute value (-20.6 mV) than that of P3CT-K (-14.2 mV), confirming a more dynamic stable solution system with less tendency to aggregate. We hypothesize that the bulky organic cation BA^+ could separate the neighboring polythiophene backbone and hence reduce the aggregation of P3CT in the solution. To further understand the solution to solid film transformation, top-view scanning electron microscopy (SEM) and atomic force microscopy (AFM) were performed. The SEM images clearly resolve agglomerated large particles in the P3CT-K film (Figure S2). A similar trend was found in AFM height images (Figure 1d), the P3CT-BA film exhibits smoother and more uniform surface topography, demonstrating a significant decreased surface roughness with smaller root-mean-square (RMS) (0.45 nm) relative to that of the P3CT-K film (0.91 nm), and such uniform film morphology is retained in the large-area P3CT-BA film (Figure S3).

Meanwhile, the $BA_2MA_3Pb_4I_{13}$ 2D perovskite film deposited onto P3CT-BA exhibits improved absorption (Figure S4), confirming the transparency results. We then performed steady-state photoluminescence (PL) characterization in both bottom and top excitation configurations. As shown in Figure 1e, the PL of all three films exhibit multiple peaks at different wavelengths, suggesting the presence of multi-perovskite phases at different $\langle n \rangle$ values after rapid crystallization in the RP 2D perovskite film.[28] The PL of the control $BA_2MA_3Pb_4I_{13}$ film (on bare ITO) is dominated by the 3D phase peak (≈ 740 nm), and stronger peaks of 2D phases with respect to the 3D phase are observed in both P3CT-X based films. These peaks assigned to $\langle n \rangle = 1, 2, 3, 4$, and to $\langle n \rangle = \infty$ phases are all observable, indicating a vertical phase separation in the order of $\langle n \rangle$ tends to occur from the bottom toward the top regions inside the 2D film. From both bottom and top excited PL (Figure 1e,f), the PL peak intensity of the $BA_2MA_3Pb_4I_{13}$ perovskite film on P3CT-BA is significantly decreased with a slight blue-shift relative to that on P3CT-K, suggesting the reduction of defects and more efficient charge transfer.[29] To further understand the role of P3CT-BA HTL on the charge-transport dynamics, time-resolved PL spectra were recorded (see Figure 1g and Table S1). The photoinduced carrier exhibits a relatively long average lifetime (τ_{ave}) of 9.6 ns for the film on the bare ITO substrate, and the τ_{ave} decreases when $BA_2MA_3Pb_4I_{13}$ was deposited onto the ITO substrate with an HTL (ITO/

P3CT-K: 7.9 ns, ITO/P3CT-BA: 5.3 ns), suggesting improvement of the carrier extraction in P3CT-BA/2D perovskite interfaces.[30]

In addition, to study the carrier dynamic process at the HTL/perovskite interface, we hypothesize that the HTL also plays an important role in the crystallization and growth of the 2D perovskite. As recorded by the top-view SEM (Figure S5), the film on the bare ITO substrate exhibits relatively small grain domains with surface cracks, and it displays increased crystal size with reduced surface cracks after depositing onto P3CT-X, especially in the case of P3CT-BA. This observation was also confirmed by AFM (Figure 2a–c), which is attributed to a more hydrophilic surface as well as the anchoring effect of the P3CT-BA HTL. The smooth surface, large and uniform grain size and surface of the 2D perovskite film suggests few defects and non-radiative recombination centers. To further elucidate the crystal orientation and vertical alignment of the 2D perovskite film, grazing incidence wide-angle X-ray scattering (GIWAXS) was introduced. As shown in Figure 2d–f, all GIWAXS patterns exhibit typical strong scattering features of crystalline RP 2D perovskites. In comparison with the film on the bare substrate and P3CT-K, sharp, sporadic Bragg spots in the film on P3CT-BA were observed, indicating the improvement of crystal packing and orientation.[2] Moreover, a series of characteristic (060), (080) and (0100) diffractions at low q value regions (low $\langle n \rangle$ value ($\langle n \rangle \leq 2$) phase) in the P3CT-BA based film, suggesting superior crystallinity and preferential orientation with respect to the substrate and higher phase purity (Figure S6).[31–33] X-ray diffraction (XRD) was also performed (Figure S7), and characteristic diffraction peaks at 14.1° and 28.2° can be observed in all three films, which correspond to the (111) and (202) lattice planes, respectively. The two peaks of perovskite film based on P3CT-BA show higher intensity and a narrower full width at half maximum, indicating enhanced crystallinity.[34] The enhanced crystallization and vertical aligned 2D perovskite film on P3CT-BA could guarantee a more efficient carrier-transport channel between two electrodes.

In light of the above findings, as well as the results of a comprehensive understanding of different P3CT-X film properties, the schematic structures of the films deposited onto P3CT-BA are illustrated in Figure 2g. The non-uniform phase may form during the spin-coating process, after a slow post-annealing process, 2D phases and 3D phase tend to form near the bottom and top areas, respectively.[31] Meanwhile, as proved in the following part, the tailored BA^+ cation in P3CT-BA could provide an additional anchoring effect, coordinating the crystallization and vertical phase alignment. In comparison with the control sample without HTL, the 2D perovskite film with P3CT-BA exhibits modified the phase distribution with finer energy gradients along the vertical direction. As a result, the potential barriers induced by quantum wells with different $\langle n \rangle$ values could be further reduced, which is beneficial for promoting charge transport and extraction, as desired for fabricating high-efficiency and large-area photovoltaic devices.

Angew. Chem. Int. Ed. **2022**, e202205111 (3 of 10)

© 2022 Wiley-VCH GmbH
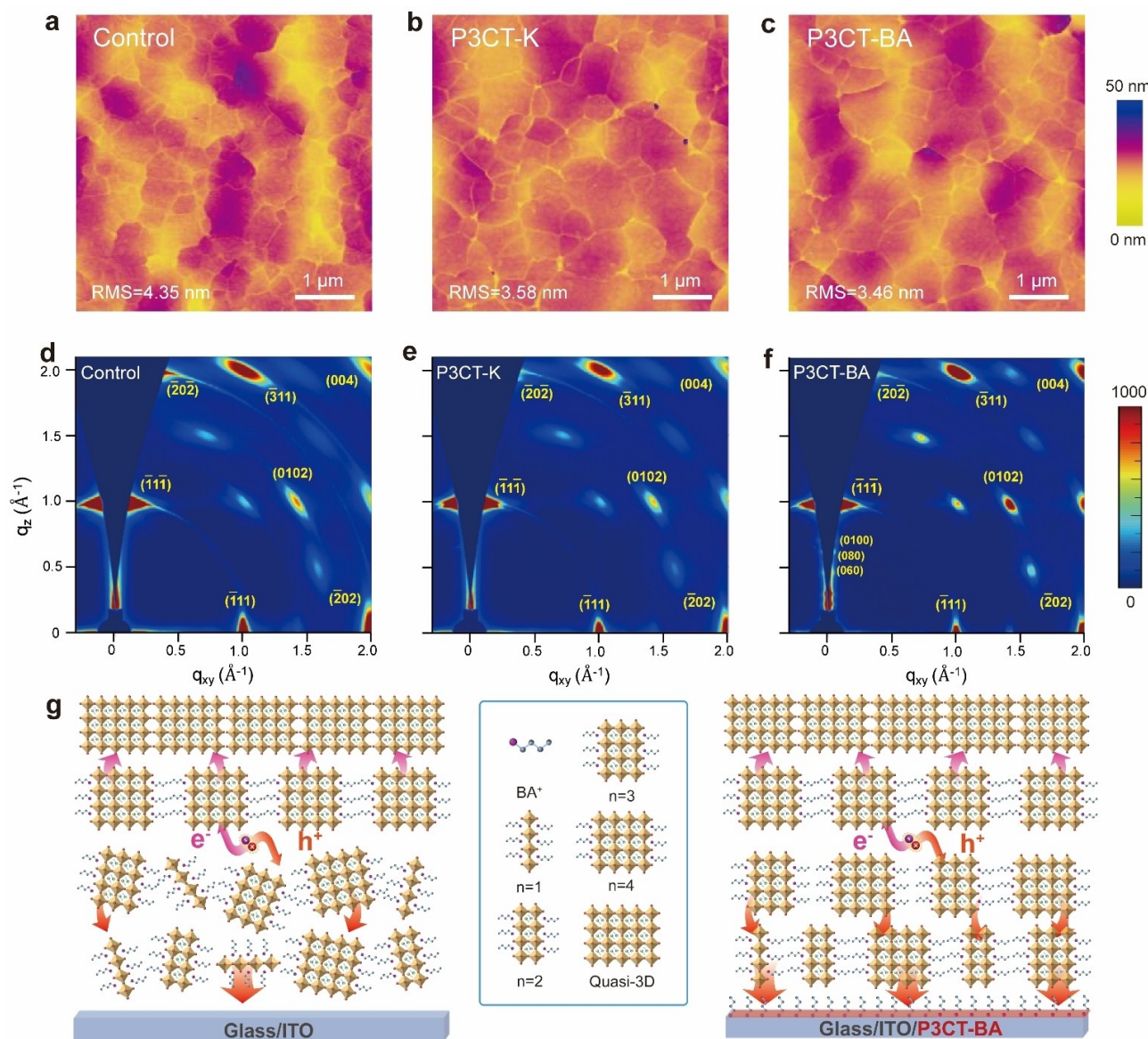
Figure 2. a)–c) AFM height images of $BA_2MA_3Pb_4I_{13}$ perovskite prepared on ITO, P3CT-K and P3CT-BA. d)–f) 2D GIWAXS patterns of $BA_2MA_3Pb_4I_{13}$ perovskite prepared on ITO, P3CT-K and P3CT-BA. g) Schematic models indicating crystal phase alignment for $BA_2MA_3Pb_4I_{13}$ perovskite films with or without P3CT-BA.

To confirm the spatial phase distribution and probe carrier transport in 2D perovskite films deposited on different substrates, femtosecond transient absorption (fs-TA) measurements were performed. Figure 3a–c present the 2D contour plots of TA spectra of quasi-2D perovskites excited from the bottom side. As expected, all the TA spectra display obvious ground-state bleaching (GSB) peaks, indicating that mixed $\langle n \rangle$ value phases coexisted in films. These GSB peaks around 560, 605, 639, 666, 725 nm can be assigned to the $\langle n \rangle = 2$, 3, 4, 5 and ∞ phases,[33,35] respectively, which is consistent with the steady PL. Figure 3d–f show the characteristics of differential transmittance (ΔOD) versus wavelength of TA, which allows for more intuitive observation of changes in GSB signals. In comparison with the control and P3CT-K-based films, the decreased relative peak intensity of the low $\langle n \rangle$ and $\langle n \rangle = \infty$ phase with respect to the $\langle n \rangle = 3$, 4, 5 phases suggest an increased homogeneity of quasi-2D phases as well as fewer unfavorable parallel phases in the P3CT-BA-based film.[1] Notably, the reduction of GSB peaks assigned to low $\langle n \rangle$ phases at higher energies are accompanied by the rise of those at $\langle n \rangle = \infty$ phases (lower energies) as the decay time prolongs, indicating an energy transfer from the low $\langle n \rangle$ to $\langle n \rangle = \infty$ phases.[36] Furthermore, by comparing the TA decay dynamics of perovskite on different substrates, we find that the decay time of the perovskite fabricated on P3CT-BA at lower $\langle n \rangle$ phases (≈ 1 ps) as well as $\langle n \rangle = \infty$ phases (≈ 100 ps) is considerably shorter than that of the control (1–10 ps and ≈ 1000 ps) and P3CT-K (1–10 ps and 1000 ps), implying faster carrier extraction time and more efficient carrier transport. In

Angew. Chem. Int. Ed. **2022**, e202205111 (4 of 10)

© 2022 Wiley-VCH GmbH
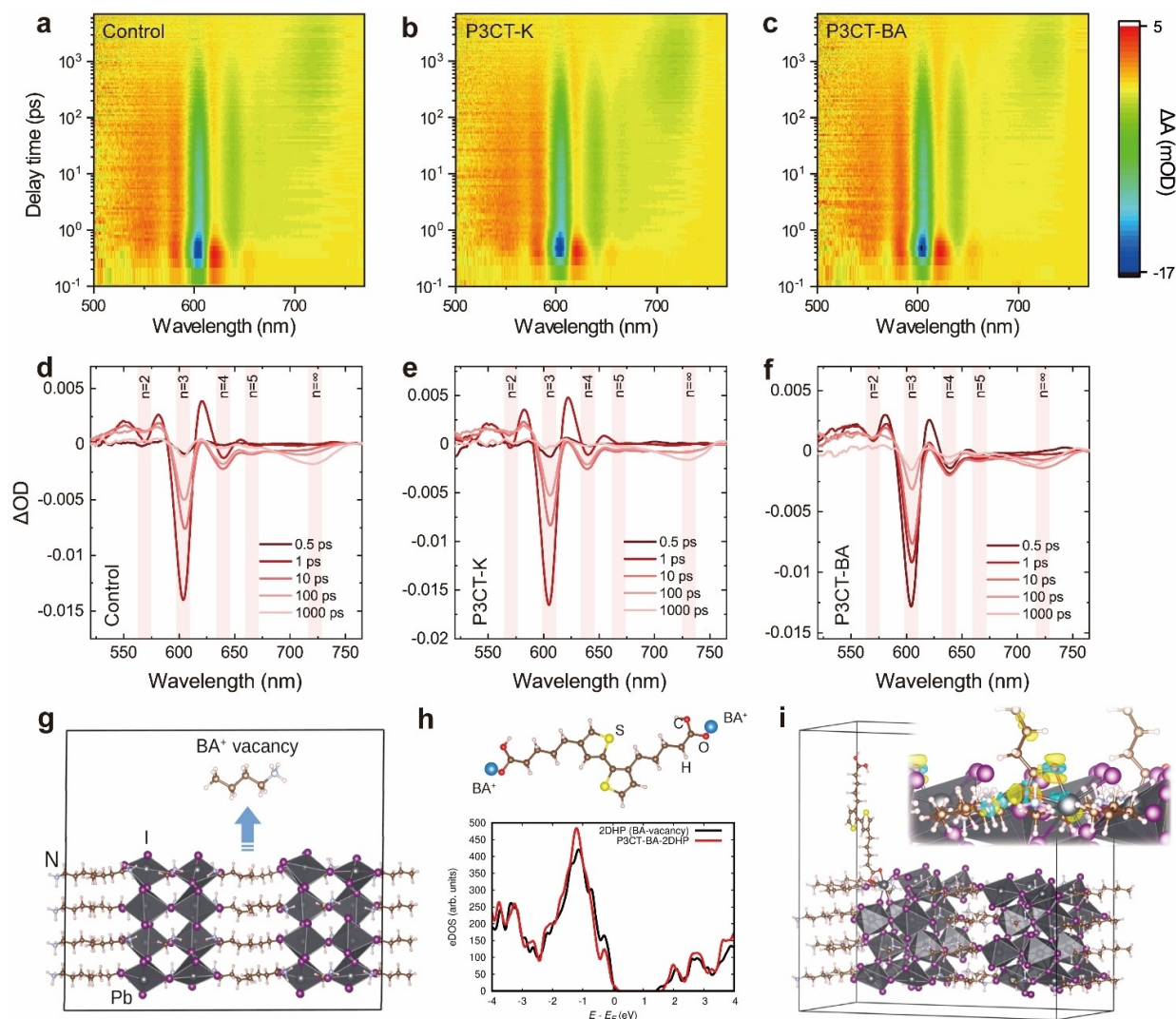
Figure 3. Transient absorption (TA) color mapping of 2D perovskite films deposited on a) ITO, b) ITO/P3CT-K and c) ITO/P3CT-BA (bottom excitation). The corresponding TA spectra at different delay times of 2D perovskite films deposited on d) ITO, e) ITO/P3CT-K and f) ITO/P3CT-BA. g) $BA_2MA_3Pb_4I_{13}$ slab system containing one BA^+ vacancy in the surface. h) Simplified P3CT-BA model employed in the DFT calculations; electronic density of states estimated for the $BA_2MA_3Pb_4I_{13}$ defected and P3CT-BA/$BA_2MA_3Pb_4I_{13}$ systems. i) Optimal P3CT-BA/$BA_2MA_3Pb_4I_{13}$ configuration and charge density difference distribution (inset: regions of electronic density accumulation (depletion) are indicated in yellow (blue)).

addition, we further fitted the TA kinetics of different phases with double-exponential functions to attain more quantitative analysis. The rising kinetics constitute a fast decay component τ_1 related to the charge transfer and a more dominant slow decay τ_2 corresponding to charge trapping process, respectively,[37] are listed in Table S2. As shown in Figure S8, it is clear that two rising kinetics of P3CT-BA-based film both become faster. Take the $\langle n \rangle = 3$ phase for example, the fitting τ_1 is 2.68, 1.55 and 0.53 ps and τ_2 is 209, 295 and 414 ps for control, P3CT-K and P3CT-BA-based perovskite films, respectively. Similar trend is also observed in other $\langle n \rangle$ value phases (Figure S8). The rising kinetics yield a shorter carrier populating time, which may be benefitted from the improved band energy and vertical phase alignment.[25]

To gain insight into the P3CT-BA/$BA_2MA_3Pb_4I_{13}$ interfaces, we performed first-principles calculations based on

density functional theory (DFT). We started by analyzing the creation of BA^+ and methylamine (MA^+) vacancies (neutral) both in bulk and surface configurations. It was found that the two types of defects entail quite similar formation energies and that it is much easier to create then in the exposed $BA_2MA_3Pb_4I_{13}$ surface (Figure 3g) than in bulk. In particular, we estimated formation energies of 2.97 (2.56) and 7.93 (7.57) eV for BA^+ (MA^+) vacancies created in the surface and interior of 2D perovskites, respectively. Subsequently, we investigated the adsorption mechanisms of a simplified molecular model for the P3CT-BA (Figure 3h) on $BA_2MA_3Pb_4I_{13}$ surfaces exclusively containing BA^+ vacancies (Figure 3i).

Upon relaxation, we observed a two-step process triggered by the adsorption of P3CT-BA like molecules that has a healing and anchoring effect on the 2D perovskite surface. First, the BA^+ moiety in one of the tips of the

Angew. Chem. Int. Ed. **2022**, e202205111 (5 of 10)

© 2022 Wiley-VCH GmbH

P3CT-BA like molecule spontaneously moves towards the vacant side in $BA_2MA_3Pb_4I_{13}$ and occupies it, thus achieving surface passivation. And second, the remainder of the P3CT-BA like molecule ends up being adsorbed on top of a surface lead (Pb) ion by its end oxygen (O) atoms, thus anchoring the perovskite surface through the creation of Pb–O bonds (Figure 3i). The total energy balance for such a molecular adsorption process renders a large binding energy of −5.98 eV, hence it is thermodynamically very favorable. The formation of Pb–O bonds in the $BA_2MA_3Pb_4I_{13}$ surface is mediated by large electronic transfers from the Pb perovskite ions to the O atoms in P3CT-BA, as shown by the charge density differences estimated for the composite P3CT-BA/$BA_2MA_3Pb_4I_{13}$ system (Figure 3i). Reassuringly, our Bader charge analysis indicates that each O atom in the lower tip of the P3CT-BA like molecule receives on average about $0.5\,e^-$ from the perovskite Pb ions. In addition, the hybrid system appears to be further stabilized via the formation of hydrogen bonds between neighboring O ions in the P3CT-BA like molecule and hydrogen ions in the

$BA_2MA_3Pb_4I_{13}$ surface. The P3CT-BA induced 2D perovskite anchoring effect, materialized through the creation of surface Pb–O bonds, may explain the observed charge extraction improvements since charge can be more easily transported through the intertwined P3CT-BA/$BA_2MA_3Pb_4I_{13}$ interface. Space-charge-limited current (SCLC) characterization was employed to confirm the buried anchoring effect of P3CT-BA (Figure S9). The perovskite film based on P3CT-BA exhibits a lower hole trap-state density of 0.84×10^{16} cm^{-3} relative to that of 1.18×10^{16} cm^{-3} for one based on P3CT-K. Besides, the μ_h significantly increases from 0.84×10^{16} cm^{2}V^{-1}s^{-1} (P3CT-K) to 3.96×10^{16} cm^{2}V^{-1}s^{-1} (P3CT-BA).

To demonstrate the potential of P3CT-BA in high-efficiency and large-area 2D PSCs, we fabricated the PSCs with a configuration of glass/ITO/P3CT-X/$BA_2MA_3Pb_4I_{13}$/(6,6)-Phenyl-C61-butyric acid methyl ester (PCBM)/Bath-ocuproine (BCP)/Ag shown in Figure 4a, with a cross-sectional SEM image shown in Figure 4b. The ultraviolet photoelectron spectroscopy (UPS) results (Figure S10) in-
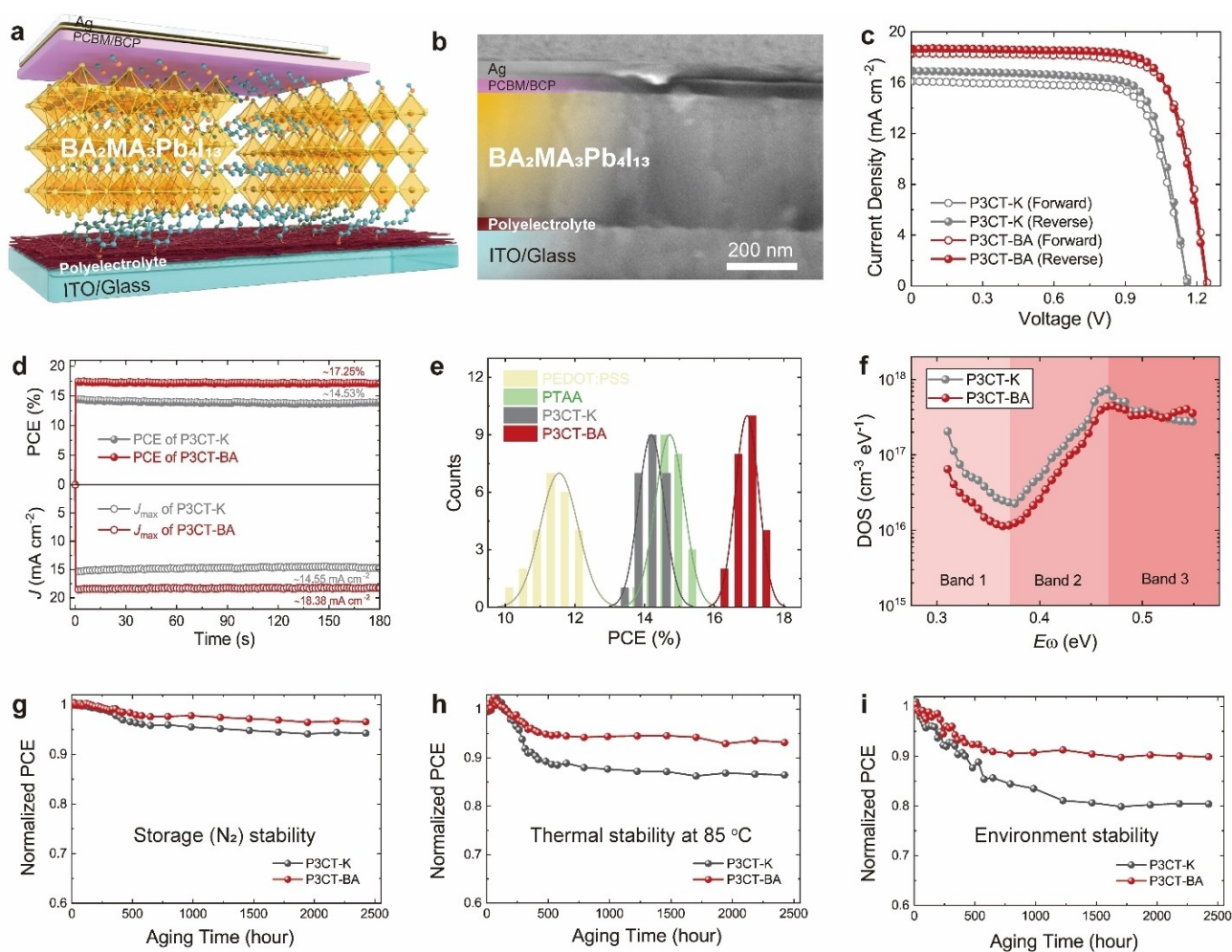
Figure 4. a) Device architecture of 2D PSCs and corresponding cross-sectional SEM image. b) The optimal *J–V* characteristics of the 2D PSCs using P3CT-K and P3CT-BA. c) SPO spectra. d) PCE distribution (24 parallel devices) of the 2D devices based on PEDOT, PTAA, P3CT-K and P3CT-BA. e) Trap density of states of the P3CT-K and P3CT-BA-based 2D PSCs. f)–h) Stability of solar cell devices based on P3CT-K and P3CT-BA under room temperature or continuous thermal stress at 85 °C under an inert atmosphere and ambient conditions.

Angew. Chem. Int. Ed. **2022**, e202205111 (6 of 10)

© 2022 Wiley-VCH GmbH

dicate that P3CT-BA has an up-shift deep HOMO of −5.2 eV relative to that of P3CT-K (−5.3 eV), which is more compatible with the ITO electrode for hole extraction (Figure S11). To optimize the device performance, adjustments were made to the P3CT/BA weight ratio, total solid concentration, and thickness (Tables S3–S5). Figure 4c presents the current density versus voltage (*J*–*V*) characteristics of the optimized 2D PSCs using P3CT-K and P3CT-BA as the HTL, with the parameters shown in Table 1. The P3CT-K based device shows a best PCE of 14.86% with a V_{oc} of 1.17 V, a J_{sc} of 16.94 mA cm^{-2}, and a fill factor (*FF*) of 0.75, while a device using P3CT-BA HTL delivers a significantly improved PCE up to 17.74% with an increased J_{sc} of 18.67 mA cm^{-2}, a V_{oc} of 1.25 V, an *FF* of 0.76 and negligible *J*–*V* hysteresis.

The steady-state output powers for the P3CT-K and P3CT-BA devices, measured under the maximum power point voltages, are 17.25% and 14.53%, respectively (Figure 4d). The external quantum efficiency (EQE) curves in Figure S12 reveal that the best P3CT-BA based cell exhibits higher EQE values across almost the whole response region. The integrated current density (*J*) values over the AM 1.5G solar spectrum for P3CT-BA and P3CT-K based cell are 18.38 mA cm^{-2} and 16.10 mA cm^{-2}, respectively, in good agreement with the J_{sc} values obtained from the *J*–*V* curves. These enhancements from EQE measurements suggest better charge transport and carrier collection in a device using P3CT-BA. Poly[bis(4-phenyl)(2,4,6-trimethylphenyl)-amine] (PTAA) is a dominate HTL in 2D PSCs,[38,39] however, the poor surface wettability of PTAA significantly limits its application in large-area device fabrication.[40,41] This is confirmed by contact angle (CA) measurements shown in Figure S13. The conventional poly(3,4-ethylene-dioxythiophene):poly(styrenesulfonate) (PEDOT:PSS) can improve the surface wettability; however, the corresponding device usually has a lower V_{oc} due to unmatched energy level.[20,42,43] Besides, the acidic property of PEDOT:PSS may lead to corrosion of both the electrode layer and perovskite active layer,[44] which will induce the degradation of PSCs (Figure S14). For a better comparison, we also fabricated the 2D PSCs using PTAA or PEDOT:PSS as the HTL under the similar device fabrication conditions (Figure S15). The P3CT-BA based device exhibits higher efficiency and better reproducibility than the P3CT-K and PTAA/PEDOT:PSS devices from the statistics of device performances (Figure 4e). Such excellent reproducibility implied

implied the improved growth of 2D perovskite films on the substrate of ITO/P3CT-BA.

To elucidate the buried passivation effect on the hole extraction and carrier dynamics in the devices, the trap density of state (*t*DOS) and light intensity dependence of J_{sc} and V_{oc} of the devices were measured. From the thermal admittance spectroscopy measurements (Figure 4f), it is obvious that the trap density of the P3CT-BA-based device is lower than that of P3CT-K at the shallow trap region (Band 1 and Band 2, 0.3–0.46 eV). To understand the charge carrier dynamics in the quasi-2D solar cell device, we measured the light intensity dependence of J_{sc} and V_{oc} of the devices. As shown in Figure S16, the α values of the P3CT-BA-based device (0.98) is slightly increased compared to that of P3CT-K (0.97), indicating a slightly decreased bimolecular recombination in devices based on P3CT-BA. For the V_{oc} measurements, the slopes of 1.21 $k_B T/q$ and 1.62 $k_B T/q$ were fitted for the devices based on P3CT-BA and P3CT-K, respectively. The lower slope value suggests that the Shockley–Read–Hall recombination has been suppressed through a polyelectrolyte anchoring effect.[45] Both measurements indicate decreased trap-state density after introducing P3CT-BA, which may be attributed to the BA$^+$ passivation (e.g., undercoordinated iodine or BA$^+$ vacancies) and O passivation (e.g., undercoordinated Pb, consistent with DFT in Figure 3i) and improved crystallinity.[46] The transient photovoltage (TPV) measurements (Figure S17) further confirmed the light intensity dependence characterization, the photovoltage decay time of the optimized P3CT-BA-based device is 430 µs, which is greatly enhanced compared to that of the device based on P3CT-K (180 µs). The electrochemical impedance spectroscopy (EIS) technique has been widely used to characterize the interfacial charge transfer and recombination. The Nyquist plots of the devices with P3CT-K and P3CT-BA as HTLs are depicted in Figure S18, with the parameters listed in Table S6. The R_{tr} of the device based on P3CT-BA exhibits a lower value of 8.86 Ω compared to that of a P3CT-K-based device (71.64 Ω), which indicates the reduction of the interfacial recombination. Meanwhile, the P3CT-BA-based device also witnesses an increase of R_{rec} (15.35 Ω) compared with the P3CT-K-based device (6.36 Ω), demonstrating more efficient interfacial charge transfer.[47]

RP phase 2D halide perovskites have been reported to exhibit excellent long-term stability relative to their 3D hybrid counterparts. Due to the enhanced crystallization

**Table 1:** PV device parameters extracted from *J*–*V* scans of devices based on P3CT-K and P3CT-BA.

Condition	Scan direction	V_{oc} [V]	J_{sc} [mA cm^{-2}]	FF	PCE [%]	HI
P3CT-K	Reverse	1.17	16.94	0.75	14.86	0.062
	Forward	1.17	16.11	0.74	13.94	
	Average[a]	1.17 ± 0.01	16.63 ± 0.31	0.74 ± 0.03	14.27 ± 0.49	
P3CT-BA	Reverse	1.25	18.67	0.76	17.74	0.030
	Forward	1.25	18.35	0.75	17.20	
	Average[a]	1.25 ± 0.01	18.45 ± 0.20	0.75 ± 0.02	17.56 ± 0.18	

[a] The data were collected among 16 cells and the cells were measured under the reverse scan.

and phase arrangement resulting from the anchoring effect, we believe that the BA cation attached to the polyelectrolyte can better stabilize the crystal lattice, thereby improving the stability of the device. We then evaluated the stability of unencapsulated devices under an N_2 environment. As shown in Figure 4g, the devices based on P3CT-K and P3CT-BA maintained 0.94 and 0.97 of their initial PCE, respectively. The thermal and humidity stability of 2D PSCs were tested and the results are shown in Figure 4h, i. After 2400 h of storage in N_2 at 85°C heating, the unencapsulated devices drop to 0.93 and 0.86 of their original PCEs for the P3CT-BA and P3CT-K-based devices, respectively. Besides, the unencapsulated P3CT-BA-based device maintains 0.90 of its initial PCE after aging 2400 h under ambient conditions ($\approx$20°C, Relative humidity = 40–50%), while the P3CT-K-based one degraded to 0.80 of its initial value over the same aging time. We speculate that P3CT-BA as HTL can affect the hydrophobicity of perovskite films. Therefore, we

measured surface contact angles with water droplets (Figure S19). We observed an apparent increase of CA for the perovskite based on P3CT-BA (65.2°) compared to that based on P3CT-K (54.3°). This means that P3CT-BA can assist to grow a perovskite film with a more hydrophobic surface, which may account for the enhanced stability under ambient environment aging.

The main goal of the P3CT-BA is to provide a better HTL/2D perovskite interface to realize efficient large-area 2D PSCs. We then fabricated large-area (2×3 and 5×5 cm^2) devices with the same structure and processing conditions as a small area device using different ITO/HTL substrates. To enable the advantages of P3CT-BA for large-area film and device, we fabricated the large-area device using a spin-coating process and the corresponding 2D perovskite films are shown in Figure 5a. We compared the images (Figure S20) and PL mapping (Figure 5b) of a 2×3 cm^2 size 2D perovskite film sample on different substrates. The P3CT-
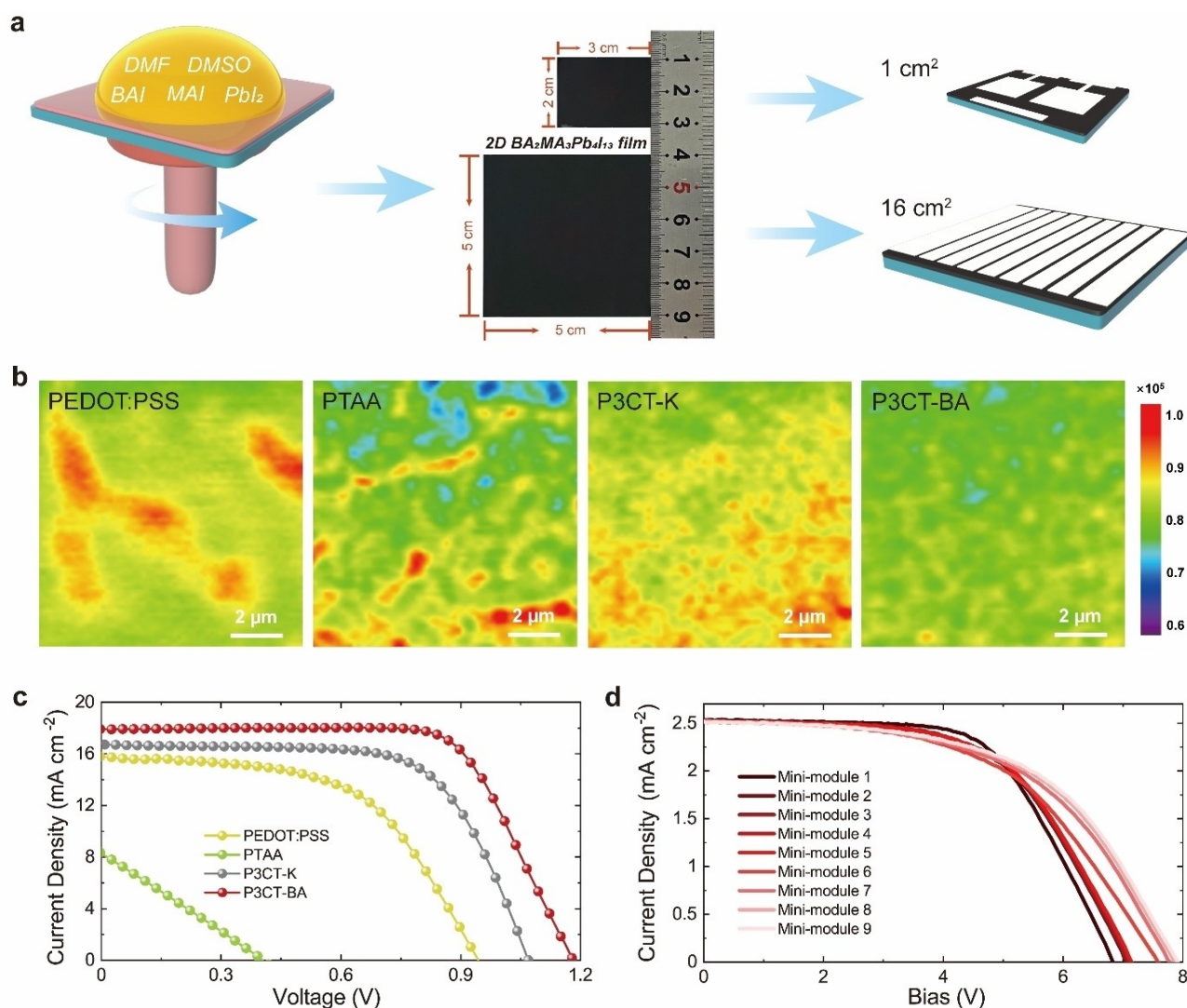
Figure 5. a) Schematic diagram of up-scaling (2×3 cm^2 and 5×5 cm^2) perovskite film fabrication. b) PL mapping of 2D perovskite films deposited on PEDOT:PSS, PTAA, P3CT-K and P3CT-BA, respectively. c) The optimal *J–V* characteristics of the 2D PSCs (1 cm^2) using PEDOT:PSS, PTAA, P3CT-K and P3CT-BA. d) The *J–V* characteristics of the 2D PSCs minimodule using P3CT-BA.

BA film shows homogeneous PL intensity, which suggests good uniformity of the large-area perovskite films. These observations were further verified by their photovoltaic performance through fabricating 1 cm^2 size device. The P3CT-BA based solar cell outputs an excellent PCE of 14.81 % (V_{oc} of 1.19 V, J_{sc} of 17.91 mA cm^{-2}, *FF* of 0.69), significantly outperforming those based on PTAA (0.86 %), PEDOT:PSS (8.26 %) and P3CT-K (11.85 %) (Figure 5c). We further evaluated the scalability of P3CT-BA by fabricating first a 2D perovskite solar module (5×5 cm^2) with a total active area of 16.00 cm^2. The module was completed by laser etching with 7 subcells. Ten minimodules using an optimal spin-coating process were fabricated and tested. Encouragingly, nine of them exhibit typical *J–V* characteristics with an average PCE of 10.53 %, and the best-performing 2D perovskite minimodule based on P3CT-BA exhibits a V_{oc} of 7.92 V, a J_{sc} of 2.51 mA cm^{-2}, an *FF* of 0.56, and a PCE of 11.13 %. This is the first 2D perovskite minimodule reported so far (Figure 5d and Table S7). Bearing the more compatible BA$^+$ cation, we believe P3CT-BA would act as a highly efficient HTL for large-scale 2D perovskite PSCs due to its great hydrophilicity, and more uniform surface. In addition, P3CT-BA also displays a buried anchoring effect to promote the growth of BA$_2$MA$_3$Pb$_4$I$_{13}$ 2D perovskite along both the horizontal and vertical directions, confirming the utility of the tailored conjugated polyelectrolyte strategy for up-scaling of 2D PSCs.

Conclusion

In summary, we report the incorporation of a functional conjugated polyelectrolyte to fabricate efficient and large-area 2D PSCs. Experimental results demonstrate that by tuning the side functional cation from K$^+$ to the compatible BA$^+$, conjugated polyelectrolyte P3CT-BA is generated which exhibits great hydrophilicity, relatively high hole mobility and a more uniform surface. The 2D PSCs using P3CT-BA as HTL exhibit enhanced charge transport and decreased trap-states, leading to a best efficiency of 17.74 % with enhanced stability, among the highest reports for 2D PSCs (Table S8). More importantly, the P3CT-BA also displays an anchoring effect and acts as the underlying passivation bottom of BA$_2$MA$_3$Pb$_4$I$_{13}$ perovskite films. The anchoring effect optimizes carrier dynamic and assists perovskite film growth, leading to a first 2D perovskite minimodule device with an efficiency of 11.13 %. We believe these results provide a feasible strategy to develop efficient, stable and large-area 2D PSCs.

Conflict of Interest

The authors declare no conflict of interest.

Data Availability Statement

The data that support the findings of this study are available from the corresponding author upon reasonable request.

[1] C. Liang, H. Gu, Y. Xia, Z. Wang, X. Liu, J. Xia, S. Zuo, Y. Hu, X. Gao, W. Hui, L. Chao, T. Niu, M. Fang, H. Lu, H. Dong, H. Yu, S. Chen, X. Ran, L. Song, B. Li, J. Zhang, Y. Peng, G. Shao, J. Wang, Y. Chen, G. Xing, W. Huang, *Nat. Energy* **2021**, *6*, 38–45.

[2] T. He, S. Li, Y. Jiang, C. Qin, M. Cui, L. Qiao, H. Xu, J. Yang, R. Long, H. Wang, M. Yuan, *Nat. Commun.* **2020**, *11*, 1672.

[3] R. Quintero-Bermudez, A. Gold-Parker, A. H. Proppe, R. Munir, Z. Yang, S. O. Kelley, A. Amassian, M. F. Toney, E. H. Sargent, *Nat. Mater.* **2018**, *17*, 900–907.

[4] J. C. Blancon, A. V. Stier, H. Tsai, W. Nie, C. C. Stoumpos, B. Traore, L. Pedesseau, M. Kepenekian, F. Katsutani, G. T. Noe, J. Kono, S. Tretiak, S. A. Crooker, C. Katan, M. G. Kanatzidis, J. J. Crochet, J. Even, A. D. Mohite, *Nat. Commun.* **2018**, *9*, 2254.

[5] Y. Lin, Y. Fang, J. Zhao, Y. Shao, S. J. Stuard, M. M. Nahid, H. Ade, Q. Wang, J. E. Shield, N. Zhou, A. M. Moran, J. Huang, *Nat. Commun.* **2019**, *10*, 1008.

[6] L. N. Quan, M. Yuan, R. Comin, O. Voznyy, E. M. Beauregard, S. Hoogland, A. Buin, A. R. Kirmani, K. Zhao, A. Amassian, D. H. Kim, E. H. Sargent, *J. Am. Chem. Soc.* **2016**, *138*, 2649–2655.

[7] N. Mercier, *Angew. Chem. Int. Ed.* **2019**, *58*, 17912–17917; *Angew. Chem.* **2019**, *131*, 18078–18083.

[8] R. Yang, R. Li, Y. Cao, Y. Wei, Y. Miao, W. L. Tan, X. Jiao, H. Chen, L. Zhang, Q. Chen, H. Zhang, W. Zou, Y. Wang, M. Yang, C. Yi, N. Wang, F. Gao, C. R. McNeill, T. Qin, J. Wang, W. Huang, *Adv. Mater.* **2018**, *30*, 1804771.

[9] H. Ren, S. Yu, L. Chao, Y. Xia, Y. Sun, S. Zuo, F. Li, T. Niu, Y. Yang, H. Ju, B. Li, H. Du, X. Gao, J. Zhang, J. Wang, L. Zhang, Y. Chen, W. Huang, *Nat. Photonics* **2020**, *14*, 154–163.

[10] G. Wu, T. Yang, X. Li, N. Ahmad, X. Zhang, S. Yue, J. Zhou, Y. Li, H. Wang, X. Shi, S. Liu, K. Zhao, H. Zhou, Y. Zhang, *Matter* **2021**, *4*, 582–599.

[11] P. Liu, N. Han, W. Wang, R. Ran, W. Zhou, Z. Shao, *Adv. Mater.* **2021**, *33*, 2002582.

[12] Y. Xu, M. Wang, Y. Lei, Z. Ci, Z. Jin, *Adv. Energy Mater.* **2020**, *10*, 2002558.

[13] H. Tsai, R. Asadpour, J. C. Blancon, C. C. Stoumpos, J. Even, P. M. Ajayan, M. G. Kanatzidis, M. A. Alam, A. D. Mohite, W. Nie, *Nat. Commun.* **2018**, *9*, 2130.

Angew. Chem. Int. Ed. **2022**, e202205111 (9 of 10)

© 2022 Wiley-VCH GmbH

[14] H. Tsai, W. Nie, J. C. Blancon, C. C. Stoumpos, R. Asadpour, B. Harutyunyan, A. J. Neukirch, R. Verduzco, J. J. Crochet, S. Tretiak, L. Pedesseau, J. Even, M. A. Alam, G. Gupta, J. Lou, P. M. Ajayan, M. J. Bedzyk, M. G. Kanatzidis, *Nature* **2016**, *536*, 312–316.

[15] S. Deng, E. Shi, L. Yuan, L. Jin, L. Dou, L. Huang, *Nat. Commun.* **2020**, *11*, 664.

[16] D. P. McMeekin, Z. Wang, W. Rehman, F. Pulvirenti, J. B. Patel, N. K. Noel, M. B. Johnston, S. R. Marder, L. M. Herz, H. J. Snaith, *Adv. Mater.* **2017**, *29*, 1607039.

[17] K. Yan, M. Long, T. Zhang, Z. Wei, H. Chen, S. Yang, J. Xu, *J. Am. Chem. Soc.* **2015**, *137*, 4460–4468.

[18] M. Jung, S. G. Ji, G. Kim, S. I. Seok, *Chem. Soc. Rev.* **2019**, *48*, 2011–2038.

[19] Y. Lin, Y. Liu, S. Chen, S. Wang, Z. Ni, C. H. Van Brackle, S. Yang, J. Zhao, Z. Yu, X. Dai, Q. Wang, Y. Deng, J. Huang, *Energy Environ. Sci.* **2021**, *14*, 1563–1572.

[20] T. Liu, Y. Jiang, M. Qin, J. Liu, L. Sun, F. Qin, L. Hu, S. Xiong, X. Jiang, F. Jiang, P. Peng, S. Jin, X. Lu, Y. Zhou, *Nat. Commun.* **2019**, *10*, 878.

[21] Y. Han, Y. Liu, J. Yuan, H. Dong, Y. Li, W. Ma, S. T. Lee, B. Sun, *ACS Nano* **2017**, *11*, 7215–7222.

[22] S. Fu, W. Zhang, X. Li, J. Guan, W. Song, J. Fang, *ACS Energy Lett.* **2021**, *6*, 3661–3668.

[23] S. Fu, X. Li, L. Wan, Y. Wu, W. Zhang, Y. Wang, Q. Bao, J. Fang, *Adv. Energy Mater.* **2019**, *9*, 1901852.

[24] X. Li, W. Zhang, Y. C. Wang, W. Zhang, H. Q. Wang, J. Fang, *Nat. Commun.* **2018**, *9*, 3806.

[25] G. Wu, X. Li, J. Zhou, J. Zhang, X. Zhang, X. Leng, P. Wang, M. Chen, D. Zhang, K. Zhao, S. F. Liu, H. Zhou, Y. Zhang, *Adv. Mater.* **2019**, *31*, 1903889.

[26] G. Wu, R. Liang, M. Ge, G. Sun, Y. Zhang, G. Xing, *Adv. Mater.* **2022**, *34*, 2105635.

[27] Y. Chang, X. Zhu, L. Zhu, Y. Wang, C. Yang, X. Gu, Y. Zhang, J. Zhang, K. Lu, X. Sun, Z. Wei, *Nano Energy* **2021**, *86*, 106098.

[28] T. Luo, Y. Zhang, Z. Xu, T. Niu, J. Wen, J. Lu, S. Jin, S. F. Liu, K. Zhao, *Adv. Mater.* **2019**, *31*, 1903848.

[29] Y. Wang, J. Yuan, X. Zhang, X. Ling, B. W. Larson, Q. Zhao, Y. Yang, Y. Shi, J. M. Luther, W. Ma, *Adv. Mater.* **2020**, *32*, 2000449.

[30] J. Yuan, X. Zhang, J. Sun, R. Patterson, H. Yao, D. Xue, Y. Wang, K. Ji, L. Hu, S. Huang, D. Chu, T. Wu, J. Hou, J. Yuan, *Adv. Funct. Mater.* **2021**, *31*, 2101272.

[31] Y. Liang, Q. Shang, Q. Wei, L. Zhao, Z. Liu, J. Shi, Y. Zhong, J. Chen, Y. Gao, M. Li, X. Liu, G. Xing, Q. Zhang, *Adv. Mater.* **2019**, *31*, 1903030.

[32] X. Zhang, R. Munir, Z. Xu, Y. Liu, H. Tsai, W. Nie, J. Li, T. Niu, D. M. Smilgies, M. G. Kanatzidis, A. D. Mohite, K. Zhao, A. Amassian, S. F. Liu, *Adv. Mater.* **2018**, *30*, 1707166.

[33] J. Liu, J. Leng, K. Wu, J. Zhang, S. Jin, *J. Am. Chem. Soc.* **2017**, *139*, 1432–1435.

[34] C. M. M. Soe, W. Nie, C. C. Stoumpos, H. Tsai, J. C. Blancon, F. Liu, J. Even, T. J. Marks, A. D. Mohite, M. G. Kanatzidis, *Adv. Energy Mater.* **2018**, *8*, 1700979.

[35] J. Song, G. Zhou, W. Chen, Q. Zhang, J. Ali, Q. Hu, J. Wang, C. Wang, W. Feng, A. B. Djurisic, H. Zhu, Y. Zhang, T. Russell, F. Liu, *Adv. Mater.* **2020**, *32*, 2002784.

[36] A. H. Proppe, R. Quintero-Bermudez, H. Tan, O. Voznyy, S. O. Kelley, E. H. Sargent, *J. Am. Chem. Soc.* **2018**, *140*, 2890–2896.

[37] R. Quintero-Bermudez, A. H. Proppe, A. Mahata, P. Todorovic, S. O. Kelley, F. De Angelis, E. H. Sargent, *J. Am. Chem. Soc.* **2019**, *141*, 13459–13467.

[38] Y. Bai, X. Meng, S. Yang, *Adv. Energy Mater.* **2018**, *8*, 1701883.

[39] T. Liu, K. Chen, Q. Hu, R. Zhu, Q. Gong, *Adv. Energy Mater.* **2016**, *6*, 1600457.

[40] W. Q. Wu, Q. Wang, Y. Fang, Y. Shao, S. Tang, Y. Deng, H. Lu, Y. Liu, T. Li, Z. Yang, A. Gruverman, J. Huang, *Nat. Commun.* **2018**, *9*, 1625.

[41] M. Stolterfoht, C. M. Wolff, J. A. Márquez, S. Zhang, C. J. Hages, D. Rothhardt, S. Albrecht, P. L. Burn, P. Meredith, T. Unold, D. Neher, *Nat. Energy* **2018**, *3*, 847–854.

[42] K.-G. Lim, S. Ahn, Y.-H. Kim, Y. Qi, T.-W. Lee, *Energy Environ. Sci.* **2016**, *9*, 932–939.

[43] W. Yan, S. Ye, Y. Li, W. Sun, H. Rao, Z. Liu, Z. Bian, C. Huang, *Adv. Energy Mater.* **2016**, *6*, 1600474.

[44] Y. Hou, H. Zhang, W. Chen, S. Chen, C. O. R. Quiroz, H. Azimi, A. Osvet, G. J. Matt, E. Zeira, J. Seuring, N. Kausch-Busies, W. Lövenich, C. J. Brabec, *Adv. Energy Mater.* **2015**, *5*, 1500543.

[45] X. Zhang, H. Huang, X. Ling, J. Sun, X. Jiang, Y. Wang, D. Xue, L. Huang, L. Chi, J. Yuan, W. Ma, *Adv. Mater.* **2022**, *34*, 2105977.

[46] Z. Ni, C. Bao, Y. Liu, Q. Jiang, W.-Q. Wu, S. Chen, X. Dai, B. Chen, B. Hartweg, Z. Yu, Z. Holman, J. Huang, *Science* **2020**, *367*, 1352–1358.

[47] D. Yang, X. Zhou, R. Yang, Z. Yang, W. Yu, X. Wang, C. Li, S. Liu, R. P. H. Chang, *Energy Environ. Sci.* **2016**, *9*, 3071–3078.

Angew. Chem. Int. Ed. **2022**, e202205111 (10 of 10)

© 2022 Wiley-VCH GmbH

Research Articles

C. Han, Y. Wang, J. Yuan, J. Sun, X. Zhang,
C. Cazorla, X. Wu, Z. Wu, J. Shi, J. Guo,
H. Huang, L. Hu, X. Liu, H. Y. Woo,
J. Yuan,* W. Ma ————— e202205111

Tailoring Phase Alignment and Interfaces
via Polyelectrolyte Anchoring Enables
Large-Area 2D Perovskite Solar Cells
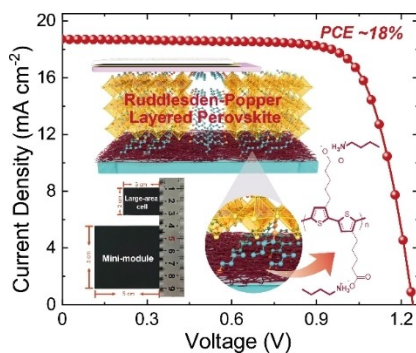
Tailored P3CT-BA polyelectrolyte is demonstrated to be an efficient hole-transporting layer for large-area 2D perovskite solar cells with a power conversion efficiency approaching 18%, and large-area (2×3 cm^2, 5×5 cm^2) 2D perovskite devices are also reported with an impressive efficiency of 14.81% and 11.13%, respectively.